

Dear Dr. Napcham

With best wishes and mco

J. Wong

BIB

SCANNING Vol. 19, 541-546 (1997)
© FAMS, Inc.

your thanks for the
I mean to use your program.

Received June 1, 1997

Accepted with revision July 23, 1997

USES MC-SET

Ferranti

Theoretical Explanation of the Relationship between Backscattered Electron and X-Ray Linear Attenuation Coefficients in Calcified Tissues

FERRANTI S. L. WONG AND JAMES C. ELLIOTT*

Department of Paediatric Dentistry, Department of Biophysics in relation to Dentistry*, Faculty of Clinical Dentistry, St. Bartholomew's and the Royal London School of Medicine and Dentistry, Queen Mary and Westfield College, London, U.K.

Summary: X-ray absorption and backscattered electron (BSE) microscopies are two commonly used techniques for estimating mineral contents in calcified tissues. The resolution in BSE images is usually higher than in x-ray images, but due to the previous lack of good standards to quantify the grey levels in BSE images of bones and teeth, x-ray microtomography (XMT) images of the same specimens have been used for calibration. However, the physics of these two techniques is different: for a specimen with a given composition, the x-ray linear attenuation coefficient is proportional to density, but there is no such relation with the BSE coefficient. To understand the reason that this calibration appears to be valid, the behaviour of simulated bone samples was investigated. In this, the bone samples were modelled as having three phases: hydroxyapatite ($\text{Ca}_{10}(\text{PO}_4)_6(\text{OH})_2$), protein, and void (either empty or completely filled with polymethylmethacrylate (PMMA), a resin which is usually used for embedding bones and teeth in microscopic studies). The x-ray linear attenuation coefficients (calculated using published data) and the BSE coefficients (calculated using Monte Carlo simulation) were compared for samples of various phase proportions. It was found that the BSE coefficient correlated only with the x-ray attenuation coefficient for samples with PMMA infiltration. This was attributed to the properties of PMMA (density and mean atomic number) being very similar to those of the protein; therefore, the sample behaves like a two-phase system which allows the establishment of a monotonic relation between density and BSE coefficient. With the newly developed standards (brominated and iodinated dimethacrylate esters) for BSE microscopy of bone, grey levels can be converted to absolute BSE coefficients by linear interpolation, from which equivalent densities can be determined.

Key words: BSE coefficient, mean atomic number, microtomography, mineral density

Introduction

Basic Principles of Backscattered Electron Microscopy

In scanning electron microscopy (SEM), images are formed using the secondary electrons (SEs) produced by interactions of the primary electron beam whose depth of penetration is ~1-5 μm below the surface of bone (Bloebaum *et al.* 1990). After penetrating the surface, the primary electrons are involved in multiple elastic and inelastic scattering events with atoms in the specimen. As a consequence, a proportion of the incident primary electrons, the backscattered electrons (BSEs), are deflected back out of the specimen. The BSE coefficient, η , is defined as the number of BSEs (n_{BSE}) divided by the number of primary beam electrons (n_p).

Monte Carlo Simulation: Monte Carlo simulation is a general statistical technique which can be used in this case to study the interactions between incident electrons and a large number of atoms within a specimen. A simulation can only be as good as the extent and quality of the experimental data on which it is based. Nevertheless, BSE coefficients obtained from Monte Carlo simulations are at least comparable with other methods of estimation (Herrmann and Reimer 1984) even though they are based on a limited database and a wide spread of values is found among various workers (Joy 1995a). The parameters needed to calculate η for an element by simulation are: the energy and the direction of the primary electron beam, the atomic number (Z), the relative atomic mass (A), and the density (ρ). For specimens of mixed elements, the mean atomic number (\bar{Z}) and mean atomic mass (\bar{A}) are used. For \bar{Z} , Lloyd (1987) used the expression:

$$\bar{Z} = \frac{\sum_{i=1}^{i=n} (NAZ)_i}{\sum_{i=1}^{i=n} (NA)_i} \quad (1)$$

where N is the number of atoms of element i in the specimen. Because $(NA)_i$ is the formula mass contribution attributable to

Address for reprints:

F. S. L. Wong
Department of Paediatric Dentistry
St. Bartholomew's and the Royal London School of Medicine and
Dentistry
Queen Mary and Westfield College
Turner Street
London, E1 2AD, U.K.

element i in the specimen with total formula mass $\sum(NA)_i$, Eq. 1 can be simplified to:

$$\bar{Z} = \sum_{i=1}^{i=n} w_i Z_i \quad (2)$$

where w_i is the mass fraction of element i , thus giving the same equation used by Müller (1954). However, there are some disputes about the summing rules for calculating the mean atomic number (Herrmann and Reimer 1984). For example, from Everhart's single scattering model (Everhart 1960), Herrmann and Reimer (1984) derived a more complex expression for \bar{Z} which was:

$$\bar{Z} = \frac{\sum_{i=1}^{i=n} w_i Z_i^2}{\sum_{i=1}^{i=n} w_i Z_i} \quad (3)$$

whereas Howell and Boyde (1994) used:

$$\bar{Z} = \frac{\sum_{i=1}^{i=n} (NZ)_i}{\sum_{i=1}^{i=n} N_i} = \sum a_i Z_i \quad (4)$$

to calculate the mean atomic number of hydroxyapatite (HAP) and polymethylmethacrylate (PMMA). Since using Eq. 2 for the mean atomic number in Monte Carlo simulations gives the closest fit of calculated η to the experimental data (Joy 1995b), it was used in this study. The mean atomic mass is also required and is given by:

$$\bar{A} = \sum_{i=1}^{i=n} w_i A_i \quad (5)$$

Linear Attenuation Coefficient: When a monochromatic x-ray beam passes through an absorbing medium, the transmitted intensity, I , obeys Beer's law, so that

$$I = I_0 \exp\left(-\int_0^z \mu(s) ds\right) \quad (6)$$

where I_0 is the incident x-ray intensity, $\mu(s)$ the linear attenuation coefficient at a distance (s) into the specimen and z the thickness. For a single-phase specimen composed of n different elements i , the following composition rule is followed:

$$\mu_m = \sum_{i=1}^{i=n} m_i \mu_{mi} \quad (7)$$

where μ_m is the mass attenuation coefficient ($\text{cm}^2 \text{g}^{-1}$) and μ_i the mass fraction of element i with mass attenuation coefficient μ_{mi} . A multiphase specimen in which individual phases are dispersed at a scale substantially smaller than the width of the beam will behave like a single-phase specimen. Thus, phases can be regarded as equivalent to elements in Eq. 7. Using the relation that $\mu_m = \mu/\rho$ where ρ is density gives

$$\mu = \sum_{i=1}^{i=n} \mu_i v_i \quad (8)$$

where v_i is the volume fraction of phase i .

The Meaning of Grey Levels in Backscattered Electron Images of Calcified Tissues

In BSE images, local variations in η are usually represented by different shades of grey colours (grey levels) or pseudo-colours. Using this technique to depict biological hard tissues, differences in grey levels have been attributed to regional variation in "mineral density" (Boyde and Jones 1983, Boyde *et al.* 1992, Fearn *et al.* 1994, Reid and Boyde 1987), "mineral content" (Reid 1986), "density" (Boyde and Reid 1983, Boyde *et al.* 1986, Mechanic *et al.* 1990, Reid 1986, Reid and Boyde 1987), and "mass density" (Burr *et al.* 1988). It has been demonstrated both experimentally (Bloebaum *et al.* 1990) and by Monte Carlo simulation (Nelson 1990) that η has a monotonic relationship with \bar{Z} (as defined in Eq. 2); thus to interpret η by terms that include "density" (it has the meaning of gravimetric density in this context) conflicts with the basic physics of the BSE imaging technique. If bone is regarded as a two-phase system comprising mineral and organic phase (including unresolvable vascular and cellular spaces), and the composition of the phases is assumed to be constant, it can be concluded from Eq. 2 that the grey levels of a BSE image represent the relative mass fraction of the two phases.

The Relation between X-Ray Linear Attenuation Coefficient and Backscattered Electron Coefficient

Although density does not appear directly in Eq. 8, it is obvious that the linear attenuation coefficient for a specimen with constant fractional elemental composition changes with its bulk density. The difference between the physics of BSE and x-ray microscopy means that the images obtained from both techniques should also be different. However, for calcified tissues, there is a striking similarity between BSE images and contact microradiographs (Nelson 1990) or x-ray microtomography (XMT) images (Fearn *et al.* 1994, Mechanic *et al.* 1990). Thus, the aim is to study this apparent conflict by comparing BSE coefficients obtained from Monte Carlo simulations with linear attenuation coefficients calculated from published data for various simulated bone specimens.

Methods

Simulation of Bone Specimens

Bone was assumed to be a three-phase mixture comprising mineral (ignoring the small amount of associated water), organic matrix, and spaces once occupied by blood vessels and cells. The mineral is taken as pure HAP, $\text{Ca}_{10}(\text{PO}_4)_6(\text{OH})_2$, with density 3.16 g cm^{-3} ; the organic matrix (Org) as protein ($\rho = 1.3 \text{ g cm}^{-3}$) with C, H, S, O, and N mass fractions of 0.525, 0.070, 0.015, 0.225, and 0.165, respectively (Weast 1976); and the space (void), assumed to be filled with air, with negligible density and elemental content. The "bone" was regarded as dehydrated and with any small amount of residual water ignored, but was embedded in polymethylmethacrylate (PMMA) with empirical formula $\text{C}_5\text{H}_8\text{O}_2$ and density 1.17 g cm^{-3} . Two groups of bone samples were simulated by varying the volume contribution of each phase. The first (Table I) and second (Table II) groups had zero, and complete infiltration of PMMA into all the voids, respectively.

Calculation of Backscattered Electron and Linear Attenuation Coefficients for the Model Bones

Using the mixture rules of Eqs. 2 and 5, the mean atomic numbers for HAP (\bar{Z}_{HAP}), organic matrix (\bar{Z}_{Org}) and PMMA (\bar{Z}_{PMMA}), and the mean atomic masses for HAP (\bar{A}_{HAP}), organic matrix (\bar{A}_{Org}) and PMMA (\bar{A}_{PMMA}) were calculated (Table III). These two equations were also used to calculate the mean atomic number and mean atomic mass for each simulated bone specimen (Tables I and II). The BSE coefficients for these samples were obtained from a Monte Carlo plural electron scattering simulation (MC-SET, Napchan 1992). The electron beam, comprising 10,000 electrons and accelerating voltage of 20 keV, was normal to the surface of the specimen.

The linear attenuation coefficients for each phase were calculated (Table III) from published mass attenuation data (McMaster *et al.* 1969) for 22.105 keV x-rays. These were used to calculate the linear attenuation coefficient for each simulated bone specimen using Eq. 8 (Tables I and II).

Results

No PMMA Infiltration

Table I gives the calculated values for samples of bone with various phase contributions, which shows

1. no relationship between η and μ (Fig. 1) or density [Fig. 2(a)];
2. an essentially linear relationship over the range studied between η and mean atomic number [Fig. 2(a)];
3. an essentially linear relationship over the range studied between μ and density [Fig. 2(b)]; and
4. no relationship between μ and mean atomic number [Fig. 2(b)].

TABLE I Calculated X-ray linear attenuation (22.105 keV) and BSE coefficients of simulated bone specimens without infiltration of PMMA. Model parameters: volume fractions of hydroxyapatite (v_{HAP}), void (v_{VOID}) and protein (v_{Org}), mean atomic number (\bar{Z}), mean atomic mass (\bar{A}), and calculated linear attenuation coefficient (μ), density (ρ) and BSE coefficient (η)

v_{HAP}	v_{VOID}	v_{Org}	\bar{Z}	\bar{A}	$\mu \text{ cm}^{-1}$	$\rho \text{ g cm}^{-3}$	η
0.8	0.2	0.0	14.06	28.31	12.19	2.53	0.168
0.3	0.7	0.0	14.06	28.31	4.57	0.95	0.162
0.1	0.9	0.0	14.06	28.31	1.52	0.32	0.163
0.8	0.1	0.1	13.69	27.53	12.26	2.65	0.157
0.5	0.4	0.1	13.48	27.10	7.69	1.71	0.159
0.5	0.2	0.3	12.55	25.16	7.82	1.97	0.152
0.5	0.1	0.4	12.17	24.37	7.88	2.10	0.142
0.3	0.2	0.5	10.95	21.84	4.91	1.60	0.132

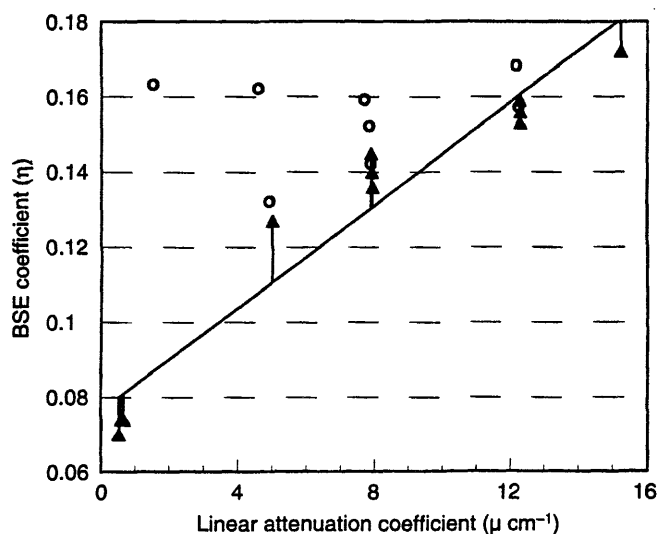


FIG. 1 The relationship between linear attenuation coefficient (22.105 keV) and backscattered electron (BSE) coefficient of simulated bones with no (○) and complete infiltration (▲) by PMMA.

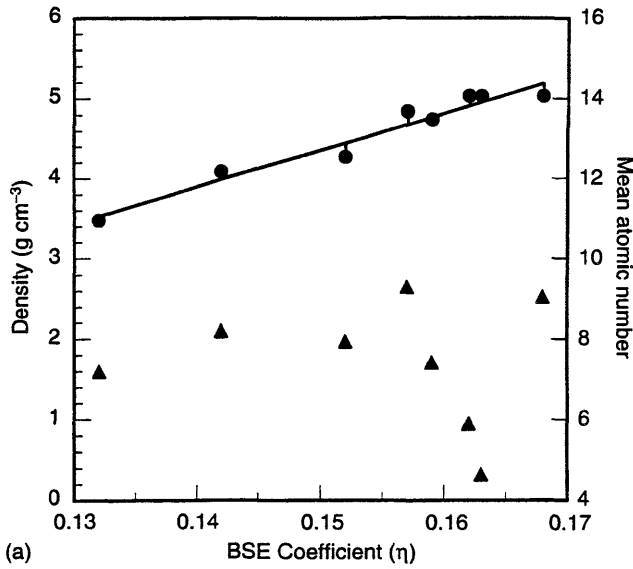
Complete PMMA Infiltration

Table II gives the calculated values for samples of bone with various phase contributions, which shows

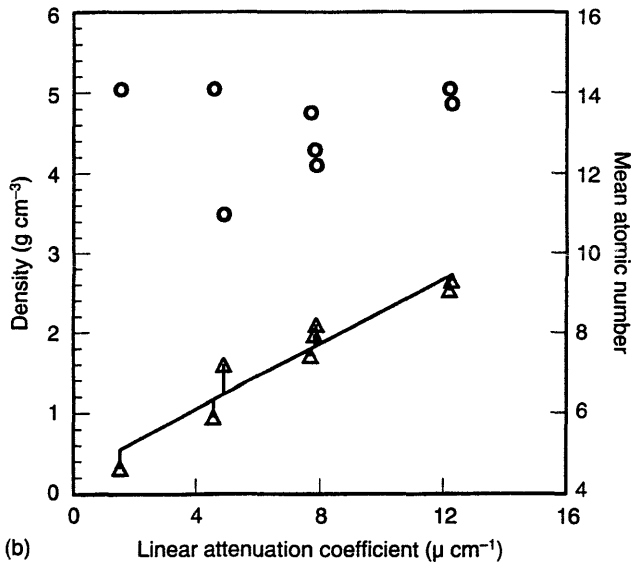
- (1) an essentially linear relationship over the range studied between η and μ (Fig. 1),
- (2) an essentially linear relationship over the range studied between η and mean atomic number, as well as density [Fig. 3(a)]; and
- (3) an essentially linear relationship over the range studied between μ and density, as well as mean atomic number [Fig. 3(b)].

Discussion

The interpretation of the grey levels in BSE images is not straightforward. As was discussed earlier, model calculations show that η depends mainly on the mean atomic number and

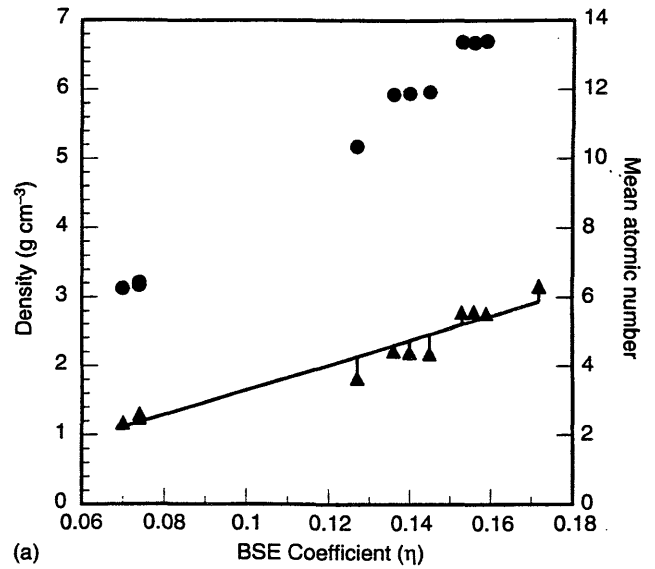


(a)

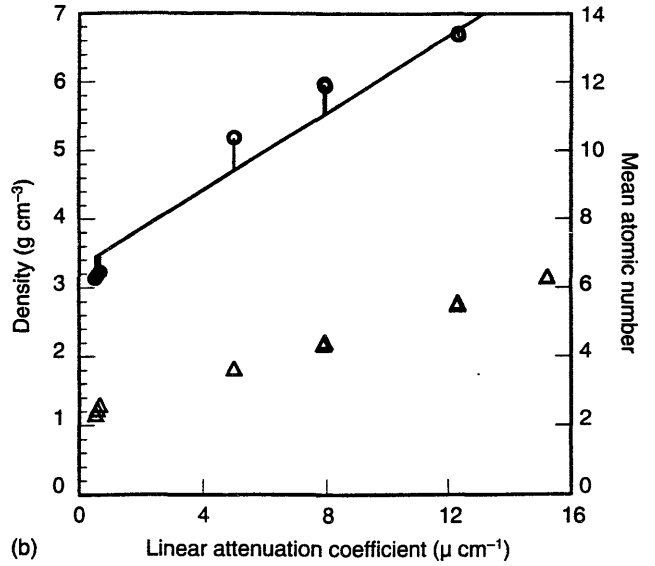


(b)

FIG. 2 No PMMA group—(a) The relationships of backscattered electron (BSE) coefficient versus density (\blacktriangle) and BSE coefficient versus mean atomic number (\bullet). The line is a linearly fitted curve to show the monotonic relation between BSE coefficient and mean atomic number. (b) The relationships of linear attenuation coefficient (22.105 keV) vs density (\triangle) and linear attenuation coefficient (22.105 keV) versus mean atomic number (\circ). The line is a linearly fitted curve to show the monotonic relation between linear attenuation coefficient and density.



(a)



(b)

FIG. 3 PMMA infiltrated group—(a) The relationships of backscattered electron (BSE) coefficient versus density (\blacktriangle) and BSE coefficient vs mean atomic number (\bullet). The line is a linearly fitted curve to show the monotonic relation between BSE coefficient and density. (b) The relationships of linear attenuation coefficient (22.105 keV) versus density (\triangle) and linear attenuation coefficient (22.105 keV) versus mean atomic number (\circ). The line is a linearly fitted curve to show the monotonic relation between linear attenuation coefficient and mean atomic number.

not on the density. Thus, it is surprising to see a marked similarity between the BSE image of a bone and its corresponding radiographic image, bearing in mind that the more x-ray opaque regions correspond to higher densities. Indeed, Skedros *et al.* (1993), using epoxy-HAP mixtures to simulate bone and measuring their BSE coefficients, showed that there was a strong relationship between density and mean atomic number. This correspondence implies that η is an increasing monotonic function of density, in apparent conflict with the

model calculations. The resolution of this conflict, as discussed below, is that the apparent relation between mean atomic number and density is only valid for two phase systems and not, in general, if more phases are present.

First consider a two-phase system with one phase in which both its mean atomic number and density are higher than the corresponding values for the other phases. The mean atomic number of the two-phase system will be given by Eq. 2 with the summation over the two phases (it is assumed these can-

TABLE II Calculated X-ray linear attenuation (22.105 keV) and BSE coefficients of simulated bone samples with infiltration of PMMA. Model parameters: volume fractions of hydroxyapatite (v_{HAP}), PMMA (v_{PMMA}) and protein (v_{Org}), mean atomic number (\bar{Z}), mean atomic mass (\bar{A}), and calculated linear attenuation coefficient (μ), density (ρ) and BSE coefficient (η)

v_{HAP}	v_{PMMA}	v_{Org}	\bar{Z}	\bar{A}	$\mu \text{ cm}^{-1}$	$\rho \text{ g cm}^3$	η
1.0	0.0	0.0	14.06	28.31	15.24	3.16	0.172
0.8	0.2	0.0	13.40	26.99	12.30	2.76	0.159
0.8	0.0	0.2	13.35	26.82	12.32	2.79	0.156
0.8	0.1	0.1	13.37	26.91	12.31	2.78	0.153
0.5	0.4	0.1	11.92	24.02	7.90	2.18	0.145
0.5	0.2	0.3	11.88	23.84	7.92	2.20	0.140
0.5	0.1	0.4	11.85	23.76	7.94	2.22	0.136
0.3	0.2	0.5	10.34	20.68	5.01	1.83	0.127
0.0	0.5	0.5	6.33	12.57	0.59	1.24	0.074
0.0	1.0	0.0	6.24	12.76	0.53	1.17	0.070
0.0	0.0	1.0	6.42	12.4	0.67	1.30	0.074

not be spatially resolved). Thus the overall η and overall density will both increase as the fraction of the phase with the higher values increases. Therefore, there will be a monotonic relation between density and η . Note, however, that if one of the phases is a vacuum, the mean atomic number calculated from Eq. 2 will be independent of the ratio of the two phases, so there will be no relation between η and density.

Now add an additional phase to give a three-phase system with the new phase chosen so that it has a higher mean atomic number, but a lower density, compared with the other two phases. If only the original two phases are now changed as before, there will still be a monotonic relation between density and η . However, if the fraction of the third phase is increased, η will increase, but the overall density will now decrease. Hence, for a general change in relative phase fractions, if η increases there might be either an increase or decrease in density. Thus, for systems comprising more than two phases, there can, in general, be no monotonic relation between η and density.

Returning to the problem of bone, it has been modelled in this work as a three-phase system comprising mineral, organic material, and space. The Monte Carlo calculations show that there is no monotonic relation between η and density. This is in accord with the above discussion. We now fill the spaces with a polymer resin, as is usual for BSE imaging, and note that the parameters that determine η and the density of the polymer are very similar to those of organic material (Table III). This means that as far as the overall η and density are concerned, the infiltrated bone behaves as a two-phase system, so there should now be a monotonic relation between η and density, as is in fact observed.

Modelling bone as a three-phase system is valid for conventional radiographic and XMT techniques because their typical resolution ($> 1 \mu\text{m}$) is not high enough to distinguish between mineral, organic matrix, and small vascular and cellular spaces. With BSE, the lateral resolution may be $< 1 \mu\text{m}$ and cellular spaces can be identified. Nevertheless, the depth of penetration of the electron varies according to the local

TABLE III Mean atomic number (\bar{Z}), mean atomic mass (\bar{A}), BSE coefficient (η), linear attenuation coefficient (μ 22.105 keV) and density (ρ) for various compounds. BrDME—brominated dimethacrylate ester, IDME—iodinated dimethacrylate ester. *From Boyde *et al.* 1995.

	\bar{Z}	\bar{A}	η	$\mu \text{ cm}^{-1}$	$\rho \text{ g cm}^3$
Hydroxyapatite	14.06	28.31	0.172	15.24	3.16
Protein	6.42	12.76	0.074	0.67	1.30
PMMA	6.24	12.40	0.070	0.53	1.17
BrDME	10.75	22.97	0.128	9.20	1.41*
IDME	16.70	37.99	0.188	7.11	1.55*

density of the sample. Therefore it can be argued that bone specimens investigated by BSE should also be considered as three-phase mixtures because of the unresolvable space under the surface of the specimen. However, since in BSE microscopy the calcified specimen is usually infiltrated with PMMA as an embedding resin, making it a pseudo two-phase system, the interpretation of the grey level variation as local variation in "mineral density" (*e.g.*, Boyde and Jones 1983, Reid and Boyde 1987) is now theoretically correct.

In XMT, the specimen is not usually embedded in resin. However, because μ_{PMMA} is so small compared with μ_{HAP} at the typical x-ray energy used, even when resin is present, its contribution to the overall linear attenuation coefficient will be so small that it is virtually the same as air. Hence, it is valid to calibrate the BSE image of a resin-infiltrated specimen by the XMT image of the same unembedded specimen, as has been done for a rat femur (Boyde *et al.* 1992) and deciduous human teeth (Fearne *et al.* 1994).

Recently, two novel brominated and iodinated dimethacrylate esters, $\text{C}_{22}\text{H}_{25}\text{O}_{10}\text{Br}$ (BrDME) and $\text{C}_{22}\text{H}_{25}\text{O}_{10}\text{I}$ (IDME), were found to be good standards for quantifying BSE images of bone (Boyde *et al.* 1995) because their grey level values straddled those for bone. This finding means that pixels in bone tissue images can now be assigned a BSE coefficient or mean atomic number. First, the mean atomic numbers, mean atomic masses, and BSE coefficient of BrDME and IDME were calculated (Table III, the densities and the linear attenuation coefficients are also listed for completeness, but not discussed here). In the paper by Boyde *et al.* (1995), the grey level values for BrDME, IDME, and bone (fetal cranial bone) peak at about 30, 225, and 120, respectively. Assuming that the grey level varies linearly with the BSE coefficient, the bone specimen has a BSE coefficient of 0.156. From the results of the model calculation [Fig. 3(a)], this corresponds to a density of about 2.3 g cm^{-3} . This value is consistent with the often quoted density of 2.0 g cm^{-3} for bone (Williams and Elliott 1989). The slightly higher value may be because we have assumed that the nonmineral/nonorganic spaces were filled with PMMA which has a density higher than for water and air.

In this study, the sequence of BSE coefficients obtained from Monte Carlo simulations for PMMA, bone, and the brominated and iodinated dimethacrylates is consistent with the experimental sequence (Boyde *et al.* 1995). This is in agreement with Howell and Boyde (1995) when they used the

same summing rule (Lloyd 1987) used here. However, using the formula $\eta = 2^{-9N/Z}$, Howell and Boyde found that only the use of the summing rule of Castaing or of Writty (both cited in Herrmann and Reimer 1984) would correctly give the sequence for PMMA, bone, and the two dimethacrylates.

Acknowledgments

The authors thank Dr. E. Napchan for the use of the MC-SET Monte Carlo Simulation program and Dr. D. Joy for his comment on BSE interactions.

References

- Bloebaum RD, Bachus KN, Boyce TM: Backscattered electron imaging: The role in calcified tissue and implant analysis. *J Biomater Appl* 5, 56-85 (1990)
- Boyde A, Jones SJ: Backscattered electron imaging of dental tissues. *Anat Embryol* 168, 211-226 (1983)
- Boyde A, Reid SA: A new method of scanning electron microscopy for imaging biological tissues. *Nature* 302, 522-523 (1983)
- Boyde A, Davy KWM, Jones SJ: Standards for mineral quantitation of human bone by analysis of backscattered electron images. *Scanning* 95, 17, 6-7 (1995)
- Boyde A, Howell PGT, Bromage TG, Elliott JC, Riggs CM, Bell LS, Kneissel M, Reid SA, Jayasinghe JAP, Jones SJ: Application of mineral quantitation of bone by histogram analysis of backscattered electron images. In *Chemistry and Biology of Mineralized Tissues*. Proceedings of the Fourth International Conference on the Chemistry and Biology of Mineralized Tissues held in Coronado, California, on February 5-9, 1992, Elsevier, Amsterdam (1992) 47-60
- Boyde A, Macconnachie E, Reid SA, Delling G, Mundy GR: Scanning electron microscopy in bone pathology: Review of methods, potential and applications. *Scan Electr Microsc* 4, 1537-1554 (1986)
- Burr DB, Schaffler MB, Frederickson RG: Composition of the cement line and its possible mechanical role as a local interface in human compact bone. *J Biomech* 21, 939-945 (1988)
- Everhart TE: Simple theory concerning the reflections of electrons from solids. *J Appl Phys* 31, 1483-1490 (1960)
- Fearne JM, Elliott JC, Wong FSL, Davis GR, Boyde A, Jones S: Deciduous enamel defects in low-birth-weight children: correlated X-ray microtomographic and backscattered electron imaging study of hypoplasia and hypomineralization. *Anat Embryol* 189, 375-381 (1994)
- Herrmann R, Reimer L: Backscattering coefficient of multicomponent specimens. *Scanning* 6, 20-29 (1984)
- Howell PGT, Boyde A: Monte Carlo simulations of electron-scattering in bone. *Bone* 15, 285-291 (1994)
- Howell PGT, Boyde A: Electron backscattering coefficients from bone. *Scanning* 17, V13-V15 (1995)
- Joy DC: A database on electron-solid interactions. *Scanning* 17, 270-275 (1995a)
- Joy DC: *Monte Carlo Modeling for Electron Microscopy and Microanalysis*. Oxford University Press, Inc., New York (1995b)
- Lloyd GE: Atomic-number and crystallographic contrast images with the SEM—a review of backscattered electron techniques. *Mineralog Mag* 51, 3-1 (1987)
- McMaster WH, Kerr Del Grande N, Mallett JH, Hubbell JH: *Compilation of X-Ray Cross Sections*. Lawrence Radiation Laboratory Report UCRL-50174 Sec.II Rev. 1 and Section IV, University of California, Livermore (1969)
- Mechanic GL, Arnaud SB, Boyde A, Bromage TG, Buckendahl P, Elliott JC, Katz EP, Durnova GN: Regional distribution of mineral and matrix in the femurs of rats flown on Cosmos 1887 biosatellite. *FASEB J* 4, 34-40 (1990)
- Müller RH: Interaction of beta particles with matter. *Phys Rev* 93, 891 (1954)
- Napchan E: Monte Carlo simulation of electron trajectories. *Microsc Anal* 32, 9-11 (1992)
- Nelson DG: Backscattered electron imaging of partially-demineralized enamel. *Scan Microsc* 4, 31-41 (1990)
- Reid SA: Effect of mineral content of human bone on in vitro resorption. *Anat Embryol* 174, 225-234 (1986)
- Reid SA, Boyde A: Changes in the mineral density distribution in human bone with age: image analysis using backscattered electrons in the SEM. *J Bone Miner Res* 2, 13-22 (1987)
- Skedros JG, Bloebaum RD, Bachus KN, Boyce TM: The meaning of gray levels in backscattered electron images of bone. *J Biomed Mater Res* 27, 47-56 (1993)
- Weast RC: *Handbook of Chemistry and Physics* (57th Ed.). CRC Press, Inc., Cleveland, Ohio (1976) E138
- Williams RAD, Elliott JC: *Basic and Applied Dental Biochemistry* (2nd Ed.). Churchill Livingstone, Edinburgh (1989)